Engineering Notes

Thermally Induced Dynamics of a Spinning Spacecraft with an Axial Flexible Boom

Zhenxing Shen* and Gengkai Hu†
Beijing Institute of Technology, 100081 Beijing, People's Republic of China

DOI: 10.2514/1.A33116

I. Introduction

SINCE the 1960s, thermally induced vibrations of spacecraft booms have been studied by many researchers [1]. Later, Thornton and Kim [2] provided an investigation on bending vibrations of the Hubble Space Telescope (HST) boom, in which the uncoupled and coupled thermal-structural analyses were presented. In addition, thermally induced attitude dynamics of a simple spacecraft as a two-dimensional structure consisting of a rigid hub and a flexible boom with tip mass was also investigated by Johnston and Thornton [3]. Recently, based on the finite element method, Xue et al. [4] examined the bending-torsion coupling vibrations of open-section booms on the HST. The aforementioned works focus on the study of a cantilevered and nonrotating boom subjected to sudden thermal loading. However, many spacecraft are spin stabilized and with large and flexible booms; therefore, study of the thermally induced dynamic motions of a spinning boom has a practical importance. An analytical study of thermally induced vibrations of a spinning boom on the Ulysses spacecraft was presented by Gulick and Thornton [5], and Ko and Kim [6] analyzed the spinning composite thin-walled beam based on the finite element method. In their studies, the boom is not connected to the spacecraft platform, therefore, thermally induced attitude dynamics of a spinning spacecraft cannot be examined.

This Note focuses on the investigation of the thermally induced attitude dynamics of a spinning spacecraft using the coupled thermal-structural analysis. A thermal analysis model of the flexible boom is first represented as a thin-walled tube, and its thermal governing equations are solved by means of the weighted residual method. For the structural analysis, the spacecraft is idealized as a rigid–flexible multibody system of a rigid hub and a cantilevered flexible boom. The natural coordinates [7] and the absolute nodal coordinate formulation [8] are employed to describe the motions of the rigid hub and flexible boom, respectively. The position vector of the boom is given by a second-order model, which can consider distortion and warping effects of beam cross section, and the elastic forces are formulated by the three-dimensional continuum mechanics approach, in which the coupling effect of tension, flexure, and torsion of a beam is included. In addition, due to the nonlinear stiffness matrix, some invariant matrices that are calculated only once in advance are also derived for saving computation time. Numerical simulations are conducted to illustrate the dynamic responses for the Ulysses spacecraft.

Received 17 July 2014; revision received 14 May 2015; accepted for publication 4 June 2015; published online 10 August 2015.

*Ph.D. Student, Key Laboratory of Dynamics and Control of Flight Vehicle, Ministry of Education, School of Aerospace Engineering; shenzhenxing_2006@126.com.

†Professor, Key Laboratory of Dynamics and Control of Flight Vehicle, Ministry of Education, School of Aerospace Engineering; hugeng@bit.edu.cn.

II. Thermal Analysis

Thermal analysis of uncoupled and coupled thermal-structural models of a spinning thin-walled tube under solar radiation is studied to determine the tube's temperature distribution. Figures 1a and 1b show, respectively, the uncoupled and coupled models, in which $\boldsymbol{S}_0$ is the solar radiation vector and β is its incident angle, one end of the tube is fixed on a rigid body and the rigid–flexible structure is rotated about X axis with a spin rate Ω, and the angle γ is dependent on the deformation of the rigid–flexible structure. Figure 1c shows the cross section of the thin-walled tube, in which R is its radius, h is its wall thickness, t is the time, $\boldsymbol{S}$ is the normal heat flux vector, and the angle φ is used to describe the points.

With the assumptions given in [5], the thermal governing equation is derived as

$$\rho c\frac{\partial T}{\partial t}-\frac{k_\varphi}{R^2}\frac{\partial^2 T}{\partial \varphi^2}+\frac{\sigma_T \varepsilon_T}{h}(T^4-T_\infty^4)=\frac{\alpha_s S}{h}\delta\cos(\varphi+\Omega t) \tag{1}$$

where ρ is the mass density, c is the specific heat, k_φ is the thermal conductivity along the circumferential direction, σ_T is the Stefan–Boltzmann constant, ε_T is the emissivity, T_∞ is the surrounding temperature, α_s is the absorptivity, S is the length of the vector $\boldsymbol{S}$, and the parameter δ is equal to one or zero [5].

Because of the discontinuity of the parameter δ, Eq. (1) is difficult to solve, therefore, the term including δ in Eq. (1) is considered by Fourier series, which is expressed as

$$\delta\cos(\varphi+\Omega t)\approx\frac{1}{\pi}+\sum_{n=1}^{M}A_n\cos n\varphi+B_n\sin n\varphi \tag{2}$$

where A_n and B_n are the Fourier coefficients, and M is the number of Fourier series.

A. Uncoupled Model

The uncoupled thermal-structural model, as shown in Fig. 1a, assumes that the absorbed solar radiation by the surface of the tube is independent of the deflection and motion of the structure. To solve Eq. (1), the temperature distribution along the circumferential direction is approximated by means of trigonometric functions and is written as

$$T(\varphi,t)\approx\bar{T}(t)+\sum_{n=1}^{M}\hat{T}_{2n-1}(t)\cos n\varphi+\hat{T}_{2n}(t)\sin n\varphi \tag{3}$$

where $\bar{T}$ is the average temperature, $\hat{T}_{2n-1}$ and $\hat{T}_{2n}$ are the perturbation temperatures, $\hat{T}_{2n-1}\ll\bar{T}$ and $\hat{T}_{2n}\ll\bar{T}$, and the value of M is the same as in Eq. (2).

Substituting Eqs. (2) and (3) into Eq. (1), then decoupling this equation by the weighted residual method and using $\cos n\varphi$ and $\sin n\varphi$ as the weight functions, respectively, one obtains

$$\begin{cases}\frac{\partial\hat{T}_{2n-1}}{\partial t}+\frac{1}{\tau_n}\hat{T}_{2n-1}=\frac{T_n^*}{\tau_n}A_n\\ \frac{\partial\hat{T}_{2n}}{\partial t}+\frac{1}{\tau_n}\hat{T}_{2n}=\frac{T_n^*}{\tau_n}B_n\end{cases} \tag{4}$$

where the integer n is from one to M, and a steady-state average temperature $\bar{T}_s$ is employed as an approximation of the transient average temperature $\bar{T}$ [2]. Thus, the parameters τ_n and T_n^* are both constant and are written, respectively, as

$$\frac{1}{\tau_n} = \frac{n^2 k}{\rho c R^2} + \frac{4\sigma_T \varepsilon_T}{\rho c h}\bar{T}_s^3 \tag{5}$$

and

$$T_n^* = \frac{\alpha_s S_0 \cos\beta}{\rho c h}\tau_n \tag{6}$$

If $n = 1$, the solution for the perturbation temperatures in Eq. (4) is

$$\begin{cases} \hat{T}_1 = \frac{T_1^*}{2(1+\Omega^2\tau_1^2)}(\cos\Omega t + \Omega\tau_1 \sin\Omega t - e^{-(t/\tau_1)}) \\ \hat{T}_2 = \frac{T_1^*}{2(1+\Omega^2\tau_1^2)}(\Omega\tau_1 \cos\Omega t - \sin\Omega t - e^{-(t/\tau_1)}) \end{cases} \tag{7}$$

and if $n > 1$, the solution of Eq. (4) is written as

$$\begin{cases} \hat{T}_{2n-1} = \hat{T}_{\max}(e^{-(t/\tau_n)} - \cos n\Omega t - n\Omega\tau_n \sin n\Omega t) \\ \hat{T}_{2n} = \hat{T}_{\max}(e^{-(t/\tau_n)} - n\Omega\tau_n \cos n\Omega t + \sin n\Omega t) \end{cases} \tag{8}$$

where

$$\hat{T}_{\max} = \frac{2T_n^* \cos(n\pi/2)}{\pi(n^2-1)(1+n^2\Omega^2\tau_n^2)} \tag{9}$$

and if n is odd except one, the perturbation temperatures are zeros.

B. Coupled Model

The coupled thermal-structural model in Fig. 1b considers the coupling effect between the normal heat flux and the structural deformations. The angle γ depends on the local coordinate x along the tube's axis direction and the time t. To solve Eq. (1), the linear interpolation functions and Eq. (3) are used to approximate the axial and circumferential temperature distributions, respectively. For one element p, the approximate temperature is given by [4]

$$T(x,\varphi,t) \approx (1-\xi)T_{p1}(\varphi,t) + \xi T_{p2}(\varphi,t) \tag{10}$$

where $\xi = x/l$, x is the element coordinate, and l is the length of the element; and the subscripts $p1$ and $p2$ denote the nodes $p1$ and $p2$, respectively.

The weight residual method is also employed, and then the element equations in a matrix form of the average and perturbation temperatures can be written, respectively, as [4]

$$\boldsymbol{C}\dot{\bar{\boldsymbol{T}}} + \bar{\boldsymbol{R}}(\bar{\boldsymbol{T}})\bar{\boldsymbol{T}} = \bar{\boldsymbol{P}}(\gamma) \tag{11}$$

and

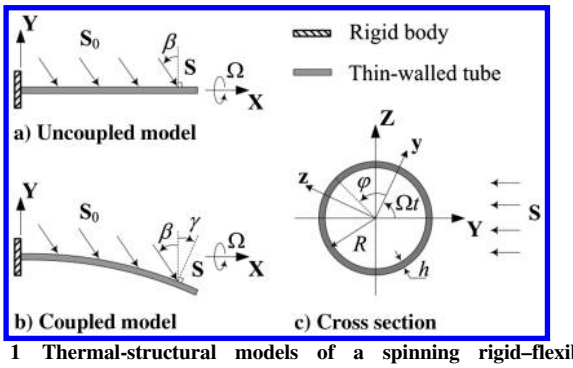

Fig. 1 Thermal-structural models of a spinning rigid–flexible multibody system.

$$\boldsymbol{C}\dot{\hat{\boldsymbol{T}}}_n + [\hat{\boldsymbol{K}}_n + 4\bar{\boldsymbol{R}}(\bar{\boldsymbol{T}})]\hat{\boldsymbol{T}}_n = \hat{\boldsymbol{P}}_n(\gamma) \tag{12}$$

where the angle γ in Eqs. (11) and (12) can be expressed as

$$\gamma = \arccos\left(\boldsymbol{n}\cdot\frac{\boldsymbol{S}_0}{|\boldsymbol{S}_0|}\right) - \beta \tag{13}$$

where $\boldsymbol{n}$ is the normal vector of the plane determined by the slope vector $\boldsymbol{r}_x$ along the tube axis and the Z axis.

III. Structural Analysis

Structural analysis of a rigid–flexible structure composed of a rigid hub and a flexible boom is presented to obtain the structural dynamic responses. The boom as a thin-walled tube beam is studied mainly by means of a three-dimensional continuum mechanics approach in the absolute nodal coordinate formulation, where the formulations of the elastic forces and the damping forces are given.

A. Elastic Forces

The position vector of a second-order model of beam cross section is employed to prevent the Poisson locking and is written as [9]

$$\begin{aligned} \boldsymbol{r} &= \boldsymbol{r}_0 + y\boldsymbol{r}_1 + z\boldsymbol{r}_2 + y^2\boldsymbol{r}_3 + yz\boldsymbol{r}_4 + z^2\boldsymbol{r}_5 \\ &= \boldsymbol{N}(x,y,z)\boldsymbol{q}(t) = \bar{\boldsymbol{q}}(t)\bar{\boldsymbol{N}}(x,y,z) \end{aligned} \tag{14}$$

where the vectors from $\boldsymbol{r}_0$ to $\boldsymbol{r}_5$ are only dependent of the element coordinate x, $\boldsymbol{N}$ is the shape function matrix, $\bar{\boldsymbol{N}}$ is its condensation, $\boldsymbol{q}$ is the nodal coordinate, and $\bar{\boldsymbol{q}}$ is the rearranged nodal coordinate. The cross-sectional distortion and warping effects can be included by the position vector [9]. For the thin-walled tube, the transverse coordinates y and z in the shape function $\boldsymbol{N}$ can be replaced by $R\cos\varphi$ and $R\sin\varphi$, respectively. In the following, the thermal effect in the elastic forces is considered and the formulation of the damping forces using this position vector is also proposed.

The virtual strain energy with thermal effect is used to formulate the elastic forces of a given element on the tube and is written as

$$\delta U = Rh\int_0^l\int_0^{2\pi}(\boldsymbol{\varepsilon}-\boldsymbol{\varepsilon}_T)^T\boldsymbol{E}\delta(\boldsymbol{\varepsilon}-\boldsymbol{\varepsilon}_T)\,\mathrm{d}x\mathrm{d}\varphi \tag{15}$$

where $\boldsymbol{E}$ is the elasticity matrix, $\boldsymbol{\varepsilon}$ is the engineering strain vector, and $\boldsymbol{\varepsilon}_T$ is the thermal strain vector, expressed as

$$\boldsymbol{\varepsilon}_T = [\alpha_T(T-T_0) \quad 0 \quad 0 \quad 0 \quad 0 \quad 0]^T \tag{16}$$

where α_T is the coefficient of thermal expansion, T_0 is the reference temperature, T is the temperature obtained by solving Eq. (1), and thermally induced axial strain is only considered. Using the position vector given in Eq. (14), the components of the engineering strain vector can be obtained, in which the normal strain ε_{xx} and the shear strain γ_{yz} are written, respectively, as [10]

$$\varepsilon_{xx} = \frac{1}{2}\left(\frac{\partial\boldsymbol{r}}{\partial x}\cdot\frac{\partial\boldsymbol{r}}{\partial x} - 1\right) = \frac{1}{2}(\bar{q}_{ij}\bar{q}_{ik}\bar{N}_j^x\bar{N}_k^x - 1) \tag{17}$$

and

$$\gamma_{yz} = \frac{\partial\boldsymbol{r}}{\partial y}\cdot\frac{\partial\boldsymbol{r}}{\partial z} = \bar{q}_{ij}\bar{q}_{ik}\bar{N}_j^y\bar{N}_k^z \tag{18}$$

where $\bar{N}_j^x$, $\bar{N}_j^y$, and $\bar{N}_k^z$ are the components of the derivatives of the matrix $\bar{\boldsymbol{N}}$ with respect to x, y, and z, respectively, and $\bar{q}_{ij}$ are the components of the matrix $\bar{\boldsymbol{q}}$. Similarly, the other normal and shear strains can be also obtained.

Submitting these strains into Eq. (15), the structural elastic forces are obtained, and its mth row is written as

$$
\begin{aligned}
(\boldsymbol{Q})_m = {} & \bar{q}_{ij}\bar{q}_{ik}\bar{q}_{uv}Rh\times \\
& \int_0^l \int_0^{2\pi} \frac{1}{2}\bar{N}_j^x \bar{N}_k^x[(\lambda+2G)\bar{N}_v^x \bar{N}_w^x + \lambda \bar{N}_v^y \bar{N}_w^y + \lambda \bar{N}_v^z \bar{N}_w^z] \\
& + \frac{1}{2}\bar{N}_j^y \bar{N}_k^y[\lambda \bar{N}_v^x \bar{N}_w^x + (\lambda+2G)\bar{N}_v^y \bar{N}_w^y + \lambda \bar{N}_v^z \bar{N}_w^z] \\
& + \frac{1}{2}\bar{N}_j^z \bar{N}_k^z[\lambda \bar{N}_v^x \bar{N}_w^x + \lambda \bar{N}_v^y \bar{N}_w^y + (\lambda+2G)\bar{N}_v^z \bar{N}_w^z] \\
& + G\bar{N}_j^x \bar{N}_k^y(\bar{N}_v^x \bar{N}_w^y + \bar{N}_v^y \bar{N}_w^x) \\
& + G\bar{N}_j^y \bar{N}_k^z(\bar{N}_v^y \bar{N}_w^z + \bar{N}_v^z \bar{N}_w^y) \\
& + G\bar{N}_j^z \bar{N}_k^x(\bar{N}_v^z \bar{N}_w^x + \bar{N}_v^x \bar{N}_w^z)\,\mathrm{d}x\mathrm{d}\varphi \\
& - \bar{q}_{uv}Rh \times \int_0^l \int_0^{2\pi} \frac{3\lambda+2G}{2}(\bar{N}_v^x \bar{N}_w^x + \bar{N}_v^y \bar{N}_w^y + \bar{N}_v^z \bar{N}_w^z)\,\mathrm{d}x\mathrm{d}\varphi
\end{aligned} \tag{19}
$$

where $m = u + 3(w-1)$, λ is the Lamé's constant, and G is the shear modulus. The mth row of the thermal elastic forces is

$$
\begin{aligned}
(\boldsymbol{Q}_T)_m = {} & \bar{q}_{uv}\alpha_T Rh\times \\
& \int_0^l \int_0^{2\pi} (T-T_0)[(\lambda+2G)\bar{N}_v^x \bar{N}_w^x + \lambda \bar{N}_v^y \bar{N}_w^y + \lambda \bar{N}_v^z \bar{N}_w^z]\,\mathrm{d}x\mathrm{d}\varphi
\end{aligned} \tag{20}
$$

According to the definition of the thermal moment M_T [5], in the temperature T, the average temperatures are not considered and $M = 1$ is adopted, because the bending deformation cannot be induced by the average temperatures and the $n > 1$ terms of the perturbation temperature part.

B. Damping Forces

Based on the Rayleigh proportional damping model, the formulation of the damping forces using the fully parameterized position vector in the absolute nodal coordinate formulation are proposed, in which the Rayleigh damping matrix is given by [11]

$$
\boldsymbol{D} = \alpha_1 \boldsymbol{M}_f + \alpha_2 \boldsymbol{K}_b \tag{21}
$$

where α_1 and α_2 are Rayleigh's parameters and depend on frequencies and damping ratio ζ, $\boldsymbol{M}_f$ is the mass matrix of the flexible boom, and $\boldsymbol{K}_b$ is the bending stiffness matrix of the flexible boom.

To formulate K_b, the position vector of Eq. (14) is separated and rewritten as

$$
\boldsymbol{r} = \boldsymbol{r}_0 + \boldsymbol{r}_b = \boldsymbol{N}_0 \boldsymbol{q} + \boldsymbol{N}_b \boldsymbol{q} \tag{22}
$$

where $\boldsymbol{r}_b$ is the part related with the transverse coordinates, and $\boldsymbol{N}_0$ and $\boldsymbol{N}_b$ are the separated shape functions. Then, the axial strain-induced bending deformation can be obtained by removing the terms not related to $\boldsymbol{r}_b$ in ε_{xx},

$$
\varepsilon_{xx}^b = \frac{1}{2}\frac{\partial \boldsymbol{r}_b}{\partial x}\cdot\frac{\partial \boldsymbol{r}_b}{\partial x} + \frac{\partial \boldsymbol{r}_0}{\partial x}\cdot\frac{\partial \boldsymbol{r}_b}{\partial x} \tag{23}
$$

The bending elastic forces can be written as

$$
\boldsymbol{Q}_b = Rh\int_0^l \int_0^{2\pi} E\varepsilon_{xx}^b \frac{\partial \varepsilon_{xx}^b}{\partial \boldsymbol{q}}\,\mathrm{d}x\mathrm{d}\varphi \tag{24}
$$

and the bending stiffness matrix can be obtained by formulating its Jacobian,

$$
\boldsymbol{K}_b = \frac{\partial \boldsymbol{Q}_b}{\partial \boldsymbol{q}} = Rh\int_0^l \int_0^{2\pi} E\frac{\partial \varepsilon_{xx}^b}{\partial \boldsymbol{q}}^{\mathrm{T}} \frac{\partial \varepsilon_{xx}^b}{\partial \boldsymbol{q}} + E\varepsilon_{xx}^b \frac{\partial^2 \varepsilon_{xx}^b}{\partial \boldsymbol{q}^2}\,\mathrm{d}x\mathrm{d}\varphi \tag{25}
$$

where E is the Young's modulus.

C. Equations of Motion

According to the principle of virtual displacements, and using the method of Lagrange multipliers, the equations of motion with the constrained conditions can be expressed as

$$
\begin{cases} \boldsymbol{M}\ddot{\boldsymbol{q}} + \boldsymbol{D}(\boldsymbol{q})\dot{\boldsymbol{q}} + \boldsymbol{Q}(\boldsymbol{q}) - \boldsymbol{Q}_T(\boldsymbol{q}) + \boldsymbol{\Phi}_q^T \boldsymbol{\lambda} = 0 \\ \boldsymbol{\Phi}(\boldsymbol{q}, t) = 0 \end{cases} \tag{26}
$$

where $\boldsymbol{\Phi}$ is the constraint matrix, $\boldsymbol{\Phi}_q$ is the Jacobian of the constraint, $\boldsymbol{\lambda}$ is the Lagrange multipliers, and $\boldsymbol{M}$ is the mass matrix assembled by the rigid hub mass matrix $\boldsymbol{M}_r$ [7] and the flexible boom mass matrix $\boldsymbol{M}_f$ [8].

IV. Numerical Results

In this section, numerical simulations are conducted to illustrate the dynamic responses of Ulysses spacecraft with an axial boom under solar radiation. Table 1 lists the geometry and material properties of the boom as a thin-walled tube, where L and v is the boom's length and the Poisson's ratio, respectively. In addition, the solar heat flux S_0 is 1390 W/m^2, the surrounding temperature T_∞ is 0 K, and the initial temperature T_0 is 290 K.

A. Validation

A classical coupled thermal-structural analysis of a cantilevered and nonrotating boom with tip mass under solar radiation is considered to verify the proposed approach. Figure 2 shows the Y displacement V over time for the boom's tip, in which the incident angle β is 80 deg, the tip mass is 1.5 kg, and the different damping ratios are considered. The results obtained by the present approach agree well with Thornton and Kim's approach [2].

B. Uncoupled Analysis of Ulysses Boom

Uncoupled thermal-structural analysis of a cantilevered spinning boom on the Ulysses spacecraft is studied, and the model is the same as in [5]. First, the results of the difference between the maximum and minimum steady-state temperatures ΔT and the steady-state temperature distributions around the boom's circumference T_{ss} [12] are shown in Figs. 3a and 3b, respectively, in which the results obtained by the different approaches are compared. FE represents the results of the finite element analysis in [12], and the results obtained by Gulick and Thornton's approach [5] is the same as the present approach in the case of $M = 1$. The results given by $M = 2$ and $M = 4$ in the present approach show a good agreement with the FE analysis.

Figure 4 shows the boom's tip paths by means of the quasi-static and dynamic analyses, respectively, in which the histories of the Y displacement V and the Z displacement W are from 0 to 500 s. For the quasi-static response, there is an excellent agreement between the present and Gulick and Thornton's [5] approaches, the tip trace under the thermal moment is a circle ring, and its period is 6 s, which is half of the spinning period of the boom. For the dynamic response, the tip trace is oscillatory near the ring, and the damping forces are not taken into account in the equations of motion because the vibration will disappear over time if the damping is included in the consideration. The vibrational response, which is the difference between the

Table 1 Boom's data from [5,12]

Parameter	Value	Units
L	7.5	m
R	0.011	m
h	5.15×10^{-5}	m
E	1.31×10^{11}	N/m^2
ν	0.3	— —
ρ	8250	kg/m^3
c	420	J/kg · K
k_φ	104	W/m · K
α_s	0.7	— —
α_T	1.8×10^{-5}	1/K
ε_T	0.114	— —

dynamic and quasi-static responses, is presented in Fig. 5. The difference $V_d - V_q$ and $W_d - W_q$ are the vibrational responses along the Y and Z directions, respectively, which are similar to the beating phenomenon in vibration. For the beats, there is about 90 deg phase difference between the Y and Z directions, and the period is about 40 s.

C. Coupled Analysis of Ulysses

A simplified model of the Ulysses spacecraft consisting of a rigid hub and a flexible boom, as shown in Fig. 6, is studied by means of the coupled thermal-structural analysis. In the rigid–flexible model, the rigid hub is a cylinder with the radius R_r of 3.2 m, the height h_r of 2.1 m, and the mass of 340 kg; θ_X, θ_Y, and θ_Z are the angles between the axis of the rigid hub and the X, Y, and Z axes, respectively; the flexible boom is subjected to the solar radiation, but that is not suddenly increased, which is the same as in [5]. At the initial time, the analysis assumes that the axis of the rigid hub is overlapped with the X axis, the axial boom has a deflection that is determined by the steady-state analysis of a cantilevered boom, and the rigid–flexible structure is rotating about X axis and has a spin rate of 5 rpm.

Figure 7 shows the traces of the boom's tip displacements and provides the responses for the different incident angles and damping ratios. For $\beta = 0$ deg, the deflection is obviously larger than $\beta = 80$ deg and is smaller than Fig. 4. For $\zeta = 0.01$, the traces will not be a perfect circle over time, which is due to the small oscillation of the rigid hub and the coupling effect between the boom's deformations and the solar heat flux. To more clearly show the histories of the displacements, the Y and Z displacements of the boom's tip, and the Y

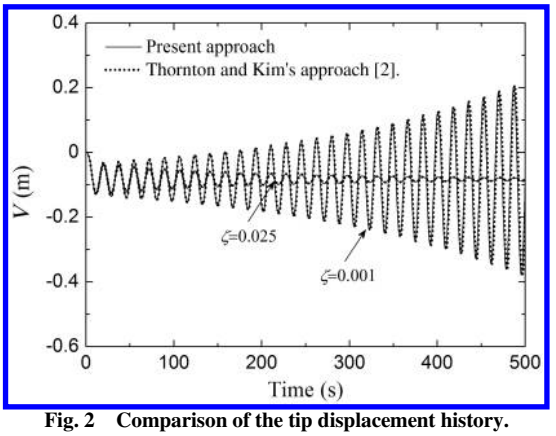

Fig. 2 Comparison of the tip displacement history.

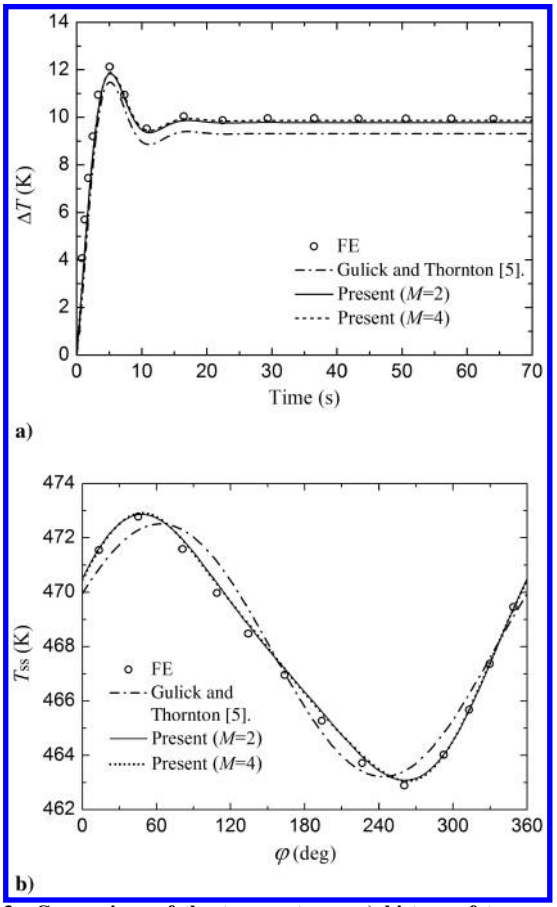

Fig. 3 Comparison of the temperatures: a) history of temperature difference and b) steady-state temperature distributions.

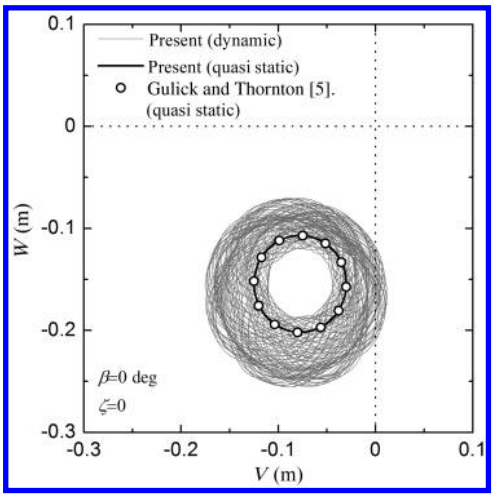

Fig. 4 Trace of tip displacements from 0 to 500 s.

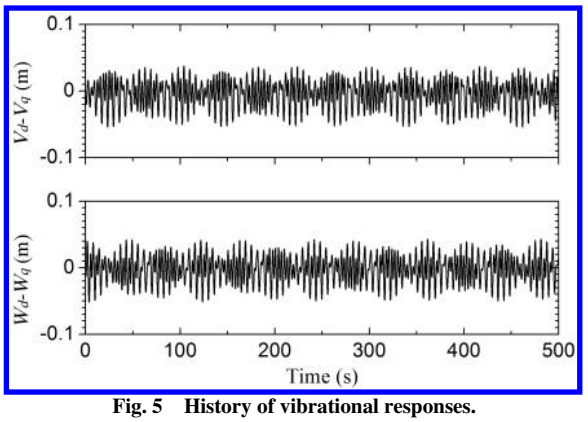

Fig. 5 History of vibrational responses.

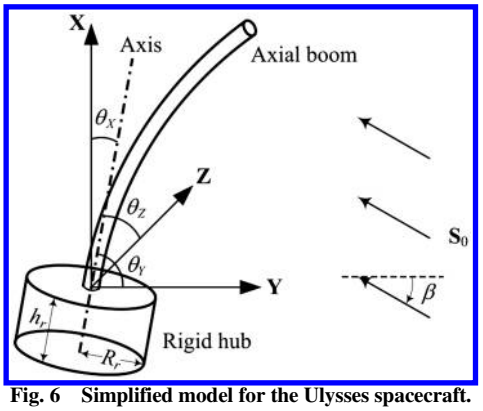

Fig. 6 Simplified model for the Ulysses spacecraft.

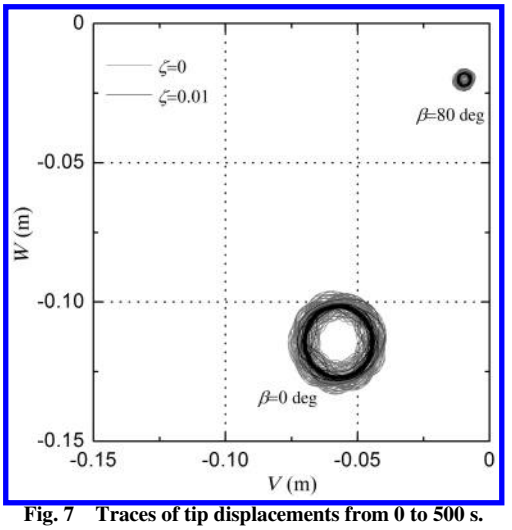

Fig. 7 Traces of tip displacements from 0 to 500 s.

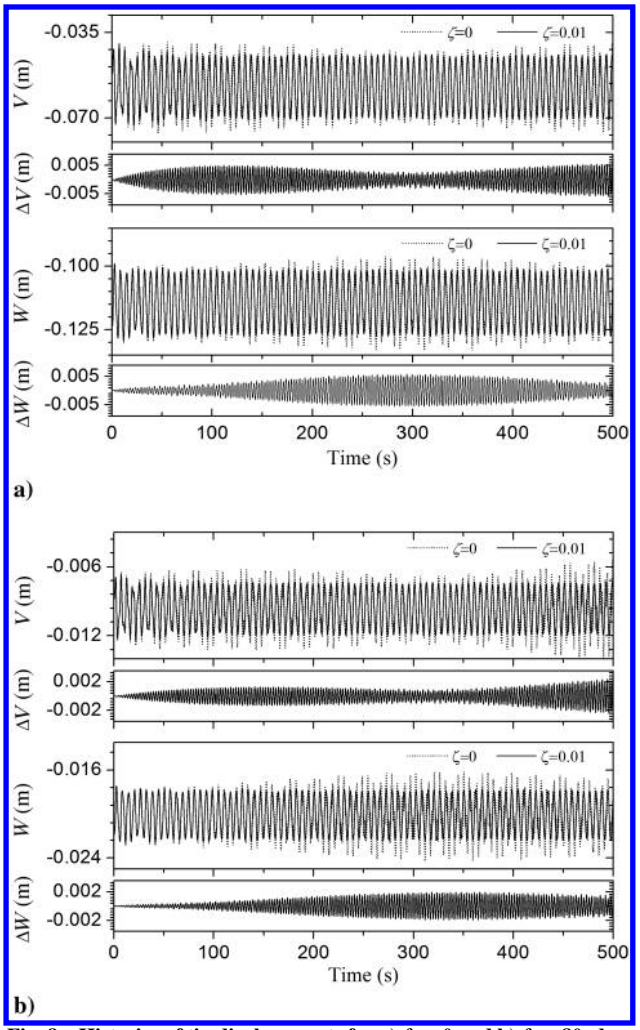

Fig. 8 Histories of tip displacements for a) $\beta = 0$ and b) $\beta = 80$ deg.

displacement difference ΔV and the Z displacement difference ΔW between $\zeta = 0$ and $\zeta = 0.01$ are also given in Fig. 8. For $\zeta = 0.01$, the vibration amplitudes of the displacements are almost invariable after about 100 s. For the displacement differences, there is a vibration characteristic that is also similar to the beating phenomenon, the periods of the beats are different between ΔV and ΔW, and the amplitudes of the beats for $\beta = 0$ deg are larger

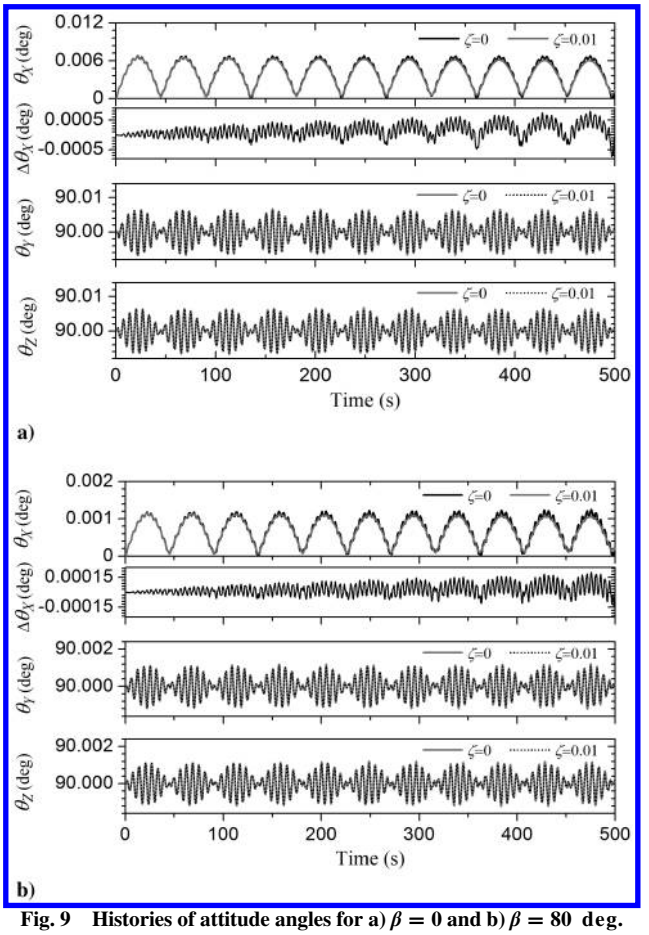

Fig. 9 Histories of attitude angles for a) $\beta = 0$ and b) $\beta = 80$ deg.

than $\beta = 80$ deg. And for ΔV in $\beta = 80$ deg, the amplitude of the beat has a significant increase.

Figure 9 shows the dynamic responses of the attitude angles θ_X, θ_Y, and θ_Z of the rigid hub, in which $\Delta\theta_X$ is the X angle difference between $\zeta = 0$ and $\zeta = 0.01$. Between $\beta = 0$ and $\beta = 80$ deg, there is no significant difference for the response shape, however, the difference for the order of magnitude is apparent. For the angle θ_X, the value is always positive because the initial thermal deformation exists in the flexible boom. For $\Delta\theta_X$, the maximum value of the envelope is increasing significantly over time, and the period of the envelope is the same as the angle θ_X. For the angles θ_Y and θ_Z, the beating characteristic is exhibited obviously, the period and phase of the beat are identical, and the period is different from Fig. 5. Between $\zeta = 0$ and $\zeta = 0.01$, there is significant difference for the angle θ_X, however, it is virtually identical for the angles θ_Y and θ_Z; because the damping forces induced by the boom's bending deformation are only considered, the damping effect of the rigid hub is not included in this simulation.

V. Conclusions

Thermally induced motions of a spinning spacecraft under solar radiation are performed by means of the absolute nodal coordinate formulation and the natural coordinates. For the uncoupled thermal analysis, the analytical solution of the temperature distribution is given, and the solution of $M = 2$ is accurate enough to describe the temperatures of the Ulysses boom. For the coupled thermal analysis, the formulation of the normal heat flux S is performed based on the boom's slope vector $\boldsymbol{r}_x$, which is easily obtained in the absolute nodal coordinate formulation. For the damping forces, the numerical results show that the proposed formulation is reasonable and accurate enough. Through numerical results, the phenomenon of the beating is observed in the attitude angles of the rigid hub on the Ulysses spacecraft.

Acknowledgments

This work was supported by the National Natural Science Foundation of China under Grants 11290153 and 11221202. The authors would like to thank Qiang Tian and Kai Zhang for their valuable suggestions.

References

[1] Thornton, E. A., and Foster, R. S., "Dynamic Response of Rapidly Heated Space Structures," *33rd Structures, Structural Dynamics and Materials Conference*, AIAA Paper 1992-2207, 1992. doi:10.2514/6.1992-2207

[2] Thornton, E. A., and Kim, Y. A., "Thermally Induced Bending Vibrations of a Flexible Rolled-Up Solar-Array," *Journal of Spacecraft and Rockets*, Vol. 30, No. 4, 1993, pp. 438–448. doi:10.2514/3.25550

[3] Johnston, J. D., and Thornton, E. A., "Thermally Induced Attitude Dynamics of a Spacecraft with a Flexible Appendage," *Journal of Guidance, Control, and Dynamics*, Vol. 21, No. 4, 1998, pp. 581–587. doi:10.2514/2.4297

[4] Xue, M. D., Duan, J., and Xiang, Z. H., "Thermally-Induced Bending-Torsion Coupling Vibration of Large Scale Space Structures," *Computational Mechanics*, Vol. 40, No. 4, 2007, pp. 707–723. doi:10.1007/s00466-006-0134-x

[5] Gulick, D. W., and Thornton, E. A., "Thermally-Induced Vibrations of a Spinning Spacecraft Boom," *Acta Astronautica*, Vol. 36, No. 3, 1995, pp. 163–176. doi:10.1016/0094-5765(95)00097-J

[6] Ko, K. E., and Kim, J. H., "Thermally Induced Vibrations of Spinning Thin-Walled Composite Beam," *AIAA Journal*, Vol. 41, No. 2, 2003, pp. 296–303. doi:10.2514/2.1943

[7] De Jalón, J. G., and Bayo, E., *Kinematic and Dynamic Simulation of Multibody System: The Real Time Challenge*, Springer–Verlag, New York, 1994, pp. 134–138.

[8] Shabana, A. A., and Yakoub, R. Y., "Three Dimensional Absolute Nodal Coordinate Formulation for Beam Elements: Theory," *Journal of Mechanical Design*, Vol. 123, No. 4, 2001, pp. 606–613. doi:10.1115/1.1410100

[9] Shen, Z., Li, P., Liu, C., and Hu, G., "A Finite Element Beam Model Including Cross-Section Distortion in the Absolute Nodal Coordinate Formulation," *Nonlinear Dynamics*, Vol. 77, No. 3, 2014, pp. 1019–1033. doi:10.1007/s11071-014-1360-y

[10] Schwab, A. L., and Meijaard, J. P., "Comparison of Three-Dimensional Flexible Beam Elements for Dynamic Analysis: Classical Finite Element Formulation and Absolute Nodal Coordinate Formulation," *Journal of Computational and Nonlinear Dynamics*, Vol. 5, No. 1, 2010, Paper 011010. doi:10.11151/1.4000320

[11] Lee, J. W., Kim, H. W., Ku, H. C., and Yoo, W. S., "Comparison of External Damping Models in a Large Deformation Problem," *Journal of Sound and Vibration*, Vol. 325, No. 4, 2009, pp. 722–741. doi:10.1016/j.jsv.2009.04.018

[12] Johnston, J. D., and Thornton, E. A., "Thermal Response of Radiantly Heated Spinning Spacecraft Booms," *Journal of Thermophysics and Heat Transfer*, Vol. 10, No. 1, 1996, pp. 60–68. doi:10.2514/3.753

D. Thunnissen
Associate Editor